POLITECNICO DI TORINO
Repository ISTITUZIONALE

Enhanced Capacitive Deionization Exploiting Novel Functionalized Graphene Oxide Electrodes

Terms of use:

Publisher copyright

(Article begins on next page)

01 September 2025

Enhanced Capacitive Deionization Exploiting Novel Functionalized Graphene Oxide Electrodes

Alessandro Pedico,* Sergio Bocchini, Elena Tresso, and Andrea Lamberti

In this study, a novel functionalized graphene oxide (fGO) is proposed for application in water desalination. The fGO is obtained with a simple and scalable method. Pristine GO is functionalized with (2-(acryloyloxy)ethyl)trimethylammonium through a two-step functionalization. Then, it is mixed with activated carbon and coated onto a metallic current collector. Material characterization techniques such as electron microscopy, thermal analyses, and infrared spectroscopy are employed to study the physical and chemical structures of the proposed materials. This process provides a porous electrode useful for capacitive deionization (CDI). The desalination performance is compared to the performance of bare activated carbons, showing a remarkable improvement. The final device reaches a value of around 17 mg g^{-1} of salt removal, with a charge efficiency of 98%. The findings from this study lay the groundwork for future research, contributing in increasing the existing knowledge on materials for CDI.

1. Introduction

The demand for freshwater worldwide is continuously increasing. Human settlements, industries, animal farms, and agriculture provide a challenge for engineers and materials' scientists to provide increasing amounts of freshwater in the most efficient and economical way. Desalination of seawater is the most feasible solution, or even the only way to supply drinkable water (H_2O) to cities, factories, and cultivated land in countries suffering scarcity of freshwater. Currently, the most widespread technology for water desalination is reverse osmosis (RO),[1] which is based on a membrane process. The energy consumption of this technology is mostly related to the high pressure (60–80 bar) required to allow the water permeation through the membranes, while rejecting the salt.[2]

A. Pedico, E. Tresso, A. Lamberti
Dipartimento di Scienza Applicata e Tecnologia (DISAT)
Politecnico di Torino
Corso Duca degli Abruzzi 24, Torino 10129, Italy
E-mail: alessandro.pedico@polito.it
S. Bocchini, A. Lamberti
Center for Sustainable Future Technologies
Istituto Italiano di Tecnologia
Via Livorno 60, Torino 10144, Italy

The ORCID identification number(s) for the author(s) of this article can be found under https://doi.org/10.1002/admt.202101513.

To lower the energy requirement of the RO process, the research is also investigating other techniques, such as nanofiltration.[3–5] Among these techniques, capacitive deionization (CDI) offers numerous advantages in terms of energy consumption, process simplicity, reduced fouling, and low cost.[6] For CDI, membrane and pressure are not required. The salt is removed by an electrical field and stored in the form of an electric double layer (EDL) in a porous medium to produce freshwater. The traditional electrodes for the capacitive technology rely on highly conductive and high-surface-area carbon-based materials.[7–10] The working principle of CDI is the same as that of a fluidic electrochemical capacitor;[11] applying a voltage to two porous electrodes immersed in a solution containing an electrolyte, the ions are attracted to the surface of the electrodes and an EDL is formed. This mechanism makes it possible to remove the salt from the water without applying any overpressure, leading to less maintenance due to the absence of mechanical moving components. Moreover, the energy is not lost in the process, but stored inside the electrodes as electrochemical energy. Therefore, it can be recovered with the very high efficiency typical of electrostatic charge storage. Unfortunately, the state of the art of this technology is still far from the performance of the more mature reverse osmosis.[7,12] New materials, providing high salt removal, low energy losses, and scalable processes, have to be developed.

In this context, functionalized materials showing a net surface charge are attracting much interest from the scientific community.[13–15] It is known that controlling the kind of the surface charge allows us to increase the desalination performance of CDI devices, because this is directly linked to the possibility of fine-tuning the potential of zero charge (V_{PZC}).[16,17] The V_{PZC} is the potential that must be applied to an electrode to ensure electroneutrality on its surface. In general, every material has its own V_{PZC} that depends on the chemical species present on its surface. For instance, graphene oxide (GO), which is constituted by carbon atoms with a high degree of oxidation, always shows a negative z-potential in water, thus having a positive V_{PZC} if used as a material for CDI electrode.

Considering the case of an electrode with $V_{PZC} > 0$ will help clarifying this concept. At equilibrium, the surface of this electrode would be populated by positive charges. Then, if a voltage greater than V_{PZC} is applied, the phenomenon known as the "co-ions' expulsion" takes place. The potential from 0 up to V_{PZC} would be used to expel the positive charges (co-ions) naturally present on the surface, while the rest ($V - V_{PZC}$) would be used to store the negative charges (counterions). Similar reasoning

ADVANCED
SCIENCE NEWS
www.advancedsciencenews.com

ADVANCED
MATERIALS
TECHNOLOGIES
www.advmattechnol.de

applies for the case of negative V_{PZC}. It is immediately clear that this situation in energetically inefficient. Part of the energy is spent to expel the co-ions, while the potential effectively used to store counterions is reduced, leading to poor salt adsorption. By contrast, if a potential of opposite sign to V_{PZC} is applied to the electrode, the co-ions' expulsion phenomenon is not taking place, since there is no change in the sign of the attracted ions. Therefore, a strategy to increase the salt absorption capacitance of the electrodes is to modify the surface of the materials with charged molecules to control their V_{PZC}. Then, coupling electrodes with opposite V_{PZC} will lead to a device with improved desalination efficiency.

GO and its reduced form (reduced graphene oxide—rGO) is a material, which has been attracting the interest of the scientific community. GO is widely reported in literature for desalination applications, mainly in form of membranes.[18,19] In the field of CDI, it is commonly used as an additive in combination with activated carbon (AC) or other carbon-based materials, as it is functionalized. In 2012, Li et al. proposed mixing AC with rGO for CDI applications. The rGO was obtained through the reduction of GO with hydrazine.[20] Two years later, Liu et al. investigated the possibility of adding a conductive agent to a carbon aerogel and then evaluated its performance in a CDI cell. For this purpose, they selected rGO as the conductive agent, in this case also obtained from the reduction of pristine GO by means of hydrazine.[21] In 2021, Folaranmi et al. used a KOH solution to reduce the GO and tested an AC/rGO compound for CDI applications.[22] In the same year, Belaustegui et al. performed CDI measurements using rGO arranged in a 3D structure and decorated with iron oxide nanoparticles.[23]

In the present work, we investigated a new kind of functionalized graphene oxide (fGO), obtained through a fast two-step functionalization procedure, which made it possible to graft a positively charged monomer on the surface of GO. We selected the (2-(acryloyloxy)ethyl)trimethylammonium chloride, a quaternary ammonium compound exhibiting a net positive charge located on the nitrogen on one side of the molecule, while, on the other side of the molecule, an ethyl acrylate group is present, which is exploited for the grafting of the monomer on the GO surface. An in-depth study was performed on the mechanism of functionalization, together with a characterization of the final material. This material is proposed for application in a CDI cell to boost the desalination efficiency of commercially available AC. The boost is obtained by directly controlling the V_{PZC} of the electrodes, shifting its value according to the charges spontaneously present on their surface or added through a functionalization procedure. The presence of the positively charged nitrogen ensures the spontaneous presence of anions (Cl^-) on the surface of the electrode. For the same purpose, unmodified GO can be used to provide negative charges thanks to the oxygen groups spontaneously present on its surface, which naturally attract cations (Na^+).

To test the effectiveness of the proposed material in CDI applications, we used two CDI cells, both made of two planar electrodes used in flow-by configuration. A symmetric device was obtained using identical electrodes. An asymmetric device was instead obtained with electrodes showing a net opposite charge. To obtain such electrodes, some crucial characteristics were carefully considered. A good adhesion of the active

material over the current collector is essential since the water flow plays a key role inside the device. Therefore, we decided to use the polyvinylidene fluoride (PVDF) as a binder, since it provides good adhesion and it is insoluble in water. As a current collector, we used titanium foil, due to its chemical stability in water. Furthermore, it is cheaper than platinum or gold. For the symmetric device, AC was chosen as an active material. The asymmetric device was made of negatively and positively charged electrodes obtained by adding, respectively, GO and fGO to the AC matrix. The direct comparison of the desalination performance of the two cells made it possible to assess the beneficial effect of the material. A significant improvement of both salt adsorption and desalination efficiency is achieved through this strategy.

2. Experimental Section

2.1. Negatively Charged Electrode Preparation

GO flakes (single-layer GO, 300–800 nm of lateral dimension, Cheap Tubes Inc.) and PVDF powder (M_w = 534 000, Sigma Aldrich) were dispersed in dimethyl sulfoxide (DMSO, ≥99.5% purity, Sigma Aldrich) in concentrations of 4 and 10 mg mL^{-1}, respectively. Both the dispersions were then sonicated for 30 min using a frequency of 59 kHz in an ultrasonic bath (LBS2, FALC INSTRUMENTS SRL). The two dispersions were mixed together, and AC power (1666 m^2 g^{-1}, MTI Corporation) was slowly added. The slurry obtained in this way was then sonicated for 30 min and stirred overnight at room temperature. The final ratio (excluded the solvent) was 90 wt% of AC, 5 wt% of PVDF, and 5 wt% of GO. No other solvents were added to the starting amount of DMSO. To obtain the final electrode, a titanium foil (0.2 mm thickness, Goodfellow) was coated with the slurry using the doctor blade method, exploiting a metallic cylinder with a spiral, whose dimension was allowed to obtain a controlled thickness of the coated film around 150 μm. The electrode as prepared was dried at 60 °C for 15 min. The dimension of the active area was 8.5 × 8.5 cm. The mass of the active material was roughly 100 mg. The edges of the electrodes were chemically and electrically insulated using a Kapton adhesive tape.

2.2. Positively Charged Electrode Preparation

The functionalization of GO flakes was based on the modification of the method described by Roppolo et al.[24] Briefly, GO flakes were dispersed in N,N-dimethylformamide (DMF, ≥99% purity, Sigma Aldrich) in a concentration of 1 mg mL^{-1}. The dispersion was sonicated for 30 min at 40 kHz. Then, 4-hydroxybenzophenone (HBP, 98% purity, Sigma Aldrich) was added to the dispersion in an amount triple with respect to the mass of the GO. The dispersion obtained in this way was stirred and bubbled in N_2 for 30 min. At this point, it was exposed to UV radiation (UV solar simulator, Newport) for 5 min with an intensity of 200 mW cm^{-2} while stirring. After this treatment, the result was an rGO functionalized with the HBP. Subsequently, the dispersion was centrifuged (IEC CL10, Thermo Scientific) at 4000 rpm for 20 min. The precipitate was washed

**ADVANCED
SCIENCE NEWS**

www.advancedsciencenews.com

**ADVANCED
MATERIALS
TECHNOLOGIES**

www.advmattechnol.de

in ethanol (anhydrous, ≥99.5% purity, Carlo Erba) and centrifuged. This step was repeated three times to separate the unreacted material. The functionalized GO obtained in this way (fGO-Step I) was dispersed again in DMF at a concentration of 2 mg mL^{-1}. To achieve the final desired functionalization, the proper amount of (2-(acryloyloxy)ethyl)trimethylammonium chloride solution (80% in H$_2$O, Sigma Aldrich) was added to the dispersion in the ratio of 5:1 with respect to fGO-Step I. The solution was stirred, degassed by nitrogen bubbling, exposed to UV, centrifuged, and washed like before. The only difference was that the exposure time was 15 min in this case. After the final washing, the fGO-Step II was obtained, and it was stored in ethanol at a concentration of 5 mg mL^{-1}. PVDF was dispersed in DMSO at a concentration of 10 mg mL^{-1} and sonicated for 30 min, like the case of the negatively charged electrode. The fGO-Step II, in ethanol, was added to the PVDF dispersion and stirred for 5 min. Then, the AC powder was slowly added and sonicated for 30 min. Finally, it was stirred overnight. As before, the final ratio of the slurry was 90 wt% AC, 5 wt% PVDF, and 5 wt% fGO-Step II. No other solvents were added to the starting amount of ethanol and DMSO. The procedure to obtain the final coated electrode was exactly the same as in the case for the negatively charged electrode.

2.3. Neutral Electrode Preparation

PVDF was dispersed in DMSO at a concentration of 5 mg mL^{-1} and then sonicated for 30 min using a frequency of 59 kHz. After the sonication step, AC was slowly added. The slurry obtained in this way was then sonicated for 30 min and stirred overnight at room temperature. The final ratio (excluded the solvent) was 90 wt% AC and 10 wt% PVDF. No other solvents were added to the starting amount of DMSO. The final electrode was undergone the same preparation procedure employed for the charged electrodes.

2.4. NaCl Solution Preparation

The sodium chloride (NaCl anhydrous, ≥99% purity, Sigma Aldrich) was dissolved in deionized water (Direct-Q 3 UV, Merck Millipore) to obtain a solution of 10×10^{-3} M in the case of capacitive deionization measurement, while 1 M in the case of electrochemical characterizations.

2.5. Characterization Techniques

Electron microscopy characterization was carried out with a field-emission scanning electron microscope (FESEM Supra 40, manufactured by Zeiss) equipped with a Si (Li) detector (Oxford Instruments) for energy-dispersive X-ray (EDX) spectroscopy.

Thermogravimetric analysis (TGA) was carried out on about 2 mg of samples using a TG 209 F1 Libra (NETZSCH GmbH), at a 20 °C min^{-1} heating rate, from 25 to 800 °C under nitrogen flow (40 cm^3 min^{-1}). The experimental error was estimated to be, by typically, less than 0.05 mg (≈± 2.5%). Gas transmittance spectra of the evolved gases were collected on a Bruker Tensor II equipped with IR gas cell (TGA–Fourier transform infrared

(FTIR) heated at 200 °C to avoid the condensation of degraded products. The instruments were coupled by Netzch FT-IR Coupling Systems transfer line heated at 230 °C. To have a stable IR background, the line was cleaned using vacuum during three cycles of vacuum/refill with nitrogen. Infrared spectra of the evolved gases were sampled at 3 °C (≈10 s) intervals. The gas development kinetics were followed at the maximum adsorption of different molecules—carbon monoxide (CO): 2179 cm^{-1}; carbon dioxide (CO$_2$): 2349 cm^{-1}; water: 3735 cm^{-1}; trimethylamine (TMA): 1267 cm^{-1}; DMF: 1716 cm^{-1}; and hydrogen chloride (HCl): 2774 cm^{-1}.

FTIR spectroscopy (Bruker Tensor II) was performed in attenuated total reflection (ATR) configuration.

Z-potential was measured by Zetasizer Nano ZS90 (Malvern) on solutions of GO with a concentration of 0.05 mg mL^{-1}.

All electrochemical characterizations were performed using the M101 Autolab (Metrohm) potentiostat with Nova 2.1 software. Conductivity measurements (Edge, Hanna Instruments) were performed during all the capacitive deionization tests.

2.6. Electrochemical Methods

The cyclic voltammetry (CV) was chosen as an electrochemical method to extract two electrochemical quantities crucial for CDI applications: the specific capacitance (C) and the Coulombic efficiency (CE). For all the materials, CV measurements were run in a 3-electrode configuration, using an Ag/AgCl 3 M KCl electrode as the reference electrode. A thick disk made of activated carbon was chosen as the counter electrode. The working electrode was made of titanium coated with the active material. The scan rate was fixed at 5 mV s^{-1}. Starting from the open-circuit potential (OCP), the potential window was increased up to ±1 V (vs OCP), with steps of 200 mV. For each potential, ten cycles were performed. The specific capacitance and the CE were evaluated from the last cycle of each CV curve. Electrochemical impedance spectroscopy (EIS) was employed to analyze the resistance behavior of different materials. The voltage signal was a sinusoid with the mean value being equal to the OCP and the peak value of 5 mV. The frequency sweep was performed from 100 kHz to 10 mHz. CV measurements were also performed on the final asymmetrical device, in a 2-electrode configuration. In this case, the voltage window was set to 1.2 V, and four different scan rates were employed: 100, 50, 10, and 5 mV s^{-1}. The last electrochemical characterization in this work was the constant current charge–discharge method. The cell was repeatedly charged up to 1.2 V and discharged down to 0 V with a current density of 0.1 A g^{-1}, and the capacitance retention was evaluated after 1000 cycles.

The specific capacitance of each material was evaluated, as reported in Equation (1)

$$C = \frac{\int I_{\text{disch}} \mathrm{d}V}{\Delta V \cdot s \cdot m} \tag{1}$$

where I_{disch} is the discharge current (A), V is the voltage over which the integration occurs (V), ΔV is the voltage window (V), s is the scan rate (V s^{-1}), and m is the mass of the active material (g).

**ADVANCED
SCIENCE NEWS**

www.advancedsciencenews.com

**ADVANCED
MATERIALS
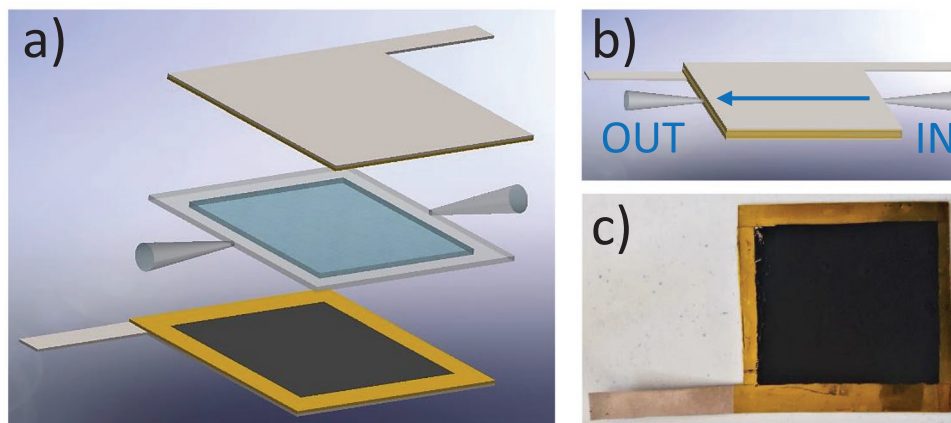TECHNOLOGIES**

www.advmattechnol.de

Figure 1. a) Exploded view of the CDI cell. On the top, an electrode with the titanium current collector on sight. In the middle, the water inside the polymeric walls defining the cell volume. On the side, the two connectors for the external tubes (inlet and outlet). On the bottom, an electrode with the active material delimited by the insulating tape. b) Compact view of the CDI cell. c) CDI electrode.

The Coulombic efficiency of each material was evaluated, as reported in Equation (2)

$$CE = \frac{\int I_{disch} dt}{\int I_{ch} dt} \qquad (2)$$

where I_{disch} is the discharge current (A), I_{ch} is the charge current (A), and t is the time over which the integration occurs (s).

2.7. CDI Measurements

The CDI tests were performed in batch mode in a homemade CDI cell (**Figure 1**a,b). The walls of the cell were the electrodes themselves (Figure 1c). The metallic finger of each electrode was used to connect the electrode to the potentiostat providing the voltage and current to the cell. The volume of the cell was defined by a polymeric spacer made of polydimethylsiloxane placed at the edges of the cell. This is a transparent, flexible and chemical inert polymer that is allowed to keep the two electrodes at a fixed distance of 1 mm. On two sides of the spacer are the inlet and the outlet. Two plastic connectors were used to connect the external tubes to them. The conductometer was placed in a separate beaker. The total volume of the solution circulating inside the system (cell + beaker) was 60 mL. A peristaltic pump (Reglo Pump, Ismatec) guaranteed a constant flux of 30 mL min⁻¹, providing a fast circulation of water from the CDI cell to the conductometer and vice versa.

The CDI tests were performed in constant flux, cyclically switching the voltage from 1.2 V (charge) to 0 V (discharge). The duration of each cycle was fixed to 10 min, with a duty cycle of 50%. Each measurement lasted for 6 h to check the process stability over time, a key feature in the CDI process.[25] The conductivity of the solution was measured once a minute.

To describe the results, three parameters were adopted, here reported following the metrics suggested by Hawks et al.[26] The maximum salt adsorption capacitance (mSAC), also called electrosorption capacity, represents the maximum amount of salt stored for each gram of active material. It was calculated measuring the conductivity and knowing the total amount of solution in the system, as reported in Equation (3)

$$mSAC = \frac{\Delta\sigma \cdot MM \cdot V}{k \cdot m} \qquad (3)$$

where $\Delta\sigma$ is the maximum conductivity variation measured during each adsorption cycle (mS cm⁻¹), MM is the molar mass of the salt (mg mol⁻¹), V is the total volume of the solution (L), k is the conversion factor from conductivity to molarity (for NaCl, 85 mS L cm⁻¹ mol⁻¹ at 25 °C), and m is the mass of the active material (g).

The charge efficiency (Λ), as described in Equation (4), is the ratio between the amounts of ions removed from the solution over the electric charge spent to do it. This charge was directly evaluated by integrating the electrical current over the charging time. It provides direct comparison of the material's efficiency, which cannot be simply evaluated from the mSAC reported in Equation (4)

$$\Lambda = \frac{mSAC \cdot F \cdot m}{MM \cdot \int I_{disch} dt} \qquad (4)$$

where F is the Faraday constant (C mol⁻¹). The third parameter used to describe the CDI result was the average salt adsorption rate (ASAR), which provides an insight into the average removal rate of salt from water stream during one cycle of operation. It is described in Equation (5)

$$ASAR = \frac{mSAC}{t_c} \qquad (5)$$

where t_c is the time of a whole cycle (min). ASAR, mSAC, and Λ are known to be the functions of the potential applied and the concentration of the solution.[27]

3. Results and Discussion

3.1. Material Characterization

In order to verify the effectiveness of the functionalization process (refer to the "Experimental Section" for further details), infrared analyses have been performed.
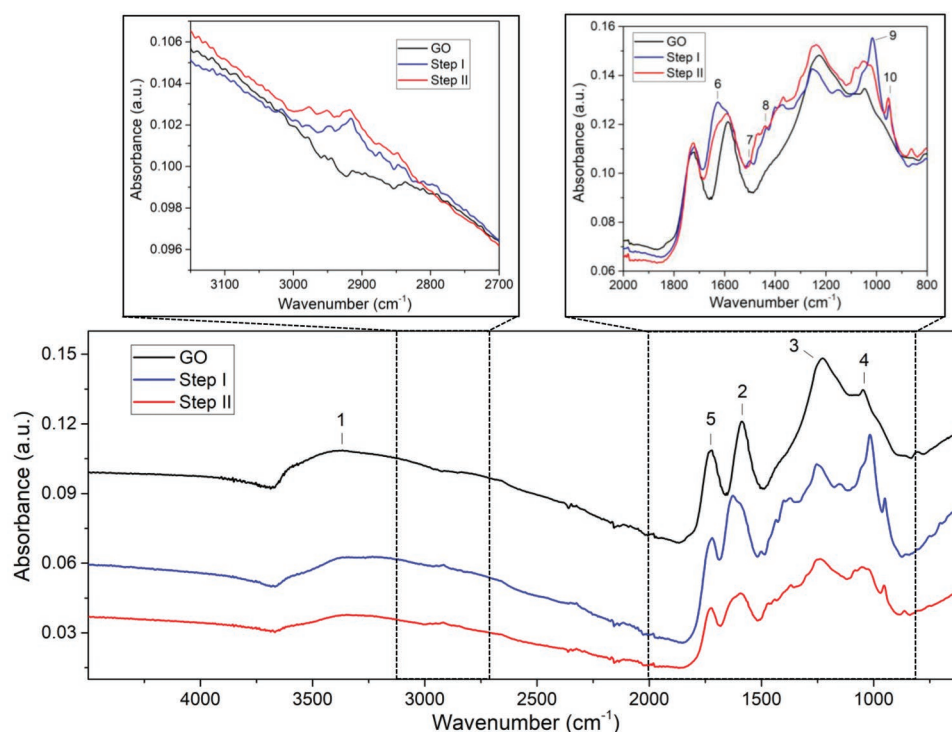
Figure 2. Fourier transform infrared (FTIR) spectra in attenuated total reflection (ATR) configuration of GO, fGO-Step I, and fGO-Step II.

The ATR spectrum of the pure GO sample has been compared with the spectra of two samples of functionalized graphene oxide, obtained after the first functionalization step (fGO-Step I, as described in the "Experimental Section") and after the second functionalization step (fGO-Step II). All the samples have been dried in order to eliminate water interference. The GO sample (**Figure 2**) shows the typical spectrum of oxidized graphene, consistently with literature.[28,29] The broad-band (1) has a maximum near 3400 cm^{-1} and corresponds to the OH stretching vibration of the hydroxyl group of alcohol and the carboxyl groups.[29,30] The band at 1586 cm^{-1} (2) is due to the deformation and vibration of aromatic C=C.[29] Epoxy groups are present at 1224 cm^{-1} (3). Alkoxy C−O has a band at 1047 cm^{-1} (4).[29,31] The band (5) with a maximum at 1718 cm^{-1} is assigned to the stretching of carbonyl C=O, mainly from carboxyl groups.[29,30]

The fGO-Step I has a similar spectrum, where the collateral presence of DMF due the functionalization procedure is evidenced by the amide I and amide III stretching bands around 1629 cm^{-1} (6) and 1504 cm^{-1} (7),[32,33] the δ_{CH2} band at 1437 cm^{-1} (8), the C−N at 1012 cm^{-1} (9) and the peak at 951 cm^{-1} (10).[34] In the C−H stretching region, the C−H absorption peaks due to the −CH₃ of DMF between 3000 and 2850 cm^{-1} are clearly visible.[32]

The fGO-Step II has similar peaks, but there are a few differences due to the presence of the grafted monomer: the peak at 1012 cm^{-1} decreases as a consequence of the degradation of the C−N group, while there is the appearance of a peak linked to C−O.[32] At higher frequencies there is an increase of absorbance in the C−H stretching region due to the methyl linked to the nitrogen of the monomer.

To clarify the type of organic substituent linked to graphene oxide, TGA has been employed as a semiqualitative analysis.

The TGA of GO (see Figure S1 in the Supporting Information) shows a main degradation peak at 220 °C, when the GO lost about 15 wt%. For temperatures varying from 330 to 800 °C, the GO slowly lost about 20 wt%, with a final residue of about 65 wt%.

The evolved gases are composed of carbon dioxide, carbon monoxide, and water. The relative intensity of their peaks does not change during the whole degradation process, following a trend similar to one of TGA first derivatives.

The TGA of fGO-Step I (see Figure S2 in the Supporting Information) shows two main degradation peaks at 190 and 366 °C. The weight losses are, respectively, 24 and 19 wt%. Successively, in the temperature interval from 500 to 800 °C, fGO-Step I lost 8 wt%, and the final residue is about 57 wt% with a difference with respect to GO of about 15 wt% on dry bases.

Infrared analysis of the evolved gases shows that the main products during the thermal degradation process are H_2O, CO, CO_2, and DMF (the latter being used as solvent during functionalization step I).[35] The molecule was probably linked to the GO by the activation created by HBP during the UV irradiation. Unfortunately, in the case of the infrared analysis, it is difficult to find traces of the HBP formation and volatilization, as reported by Roppolo et al.[24]

The TGA of fGO-Step II (**Figure 3**) shows two main degradation peaks at 190 and at 308 °C. The weight losses are about 20 wt% each. fGO-Step II lost 10 wt% from 500 to 800 °C, with a final residue of about 50 wt% and a difference with respect to GO of about 15 wt% on dry base.
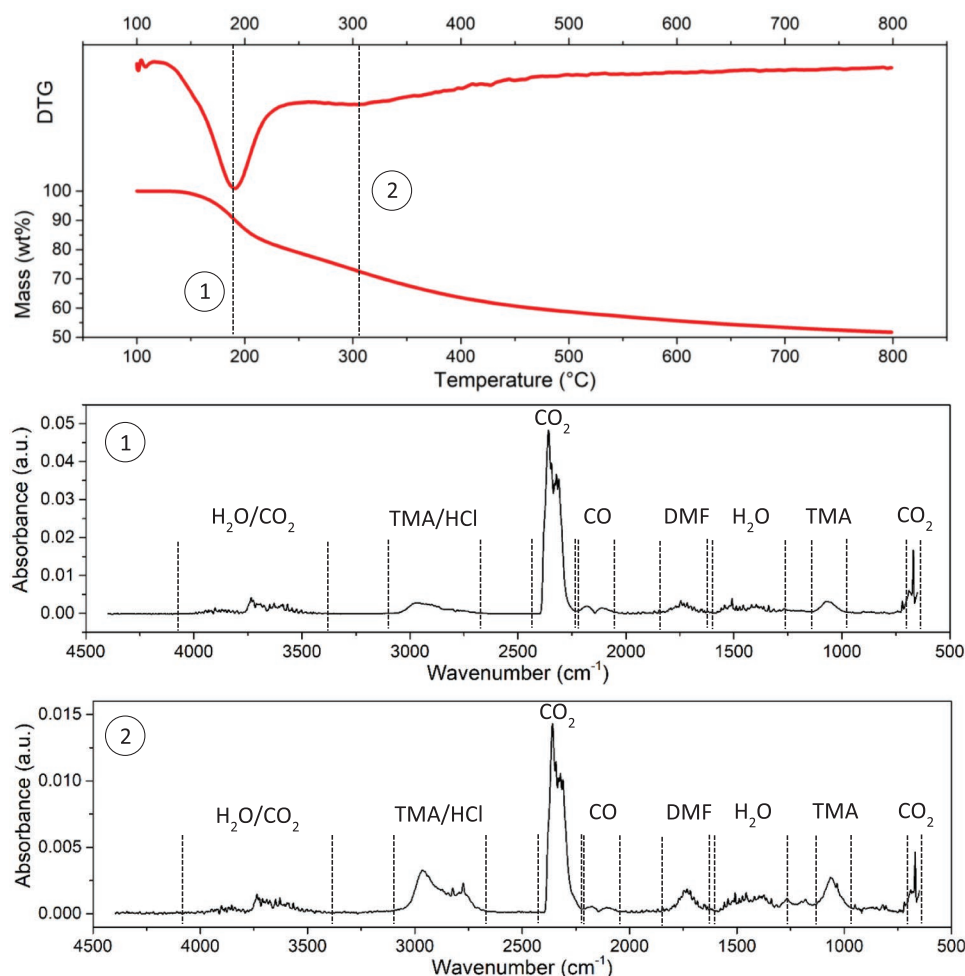
**ADVANCED
SCIENCE NEWS**

www.advancedsciencenews.com

**ADVANCED
MATERIALS
TECHNOLOGIES**

www.advmattechnol.de

Figure 3. TGA of fGO-Step II. Weight versus temperature (wt% vs °C) and differential weight versus temperature (dwt%/d°C vs °C). 1) Fourier transform infrared (FTIR) of evolved gases at 190 °C. 2) FTIR of evolved gases at 308 °C. The characteristic intervals of water (H_2O), carbon dioxide (CO_2), carbon monoxide (CO), hydrochloric acid (HCl), trimethylamine (TMA), and DMF are delimited with dashed lines.

Infrared analysis of the evolved gases shows that the main products during the first degradation process are similar to the products obtained with fGO-Step I. Infrared analyses of the evolved gases show the formation of H_2O,[36] CO,[37] and CO_2.[38] They are easily recognizable from the typical features shown in the characteristic intervals (Figure 3). In this spectrum, the DMF features are recognizable around 1730 cm^{-1}.[39] Referring to the 3D graph (temperature vs wavenumber vs absorbance) reported in **Figure 4**a, it is possible to observe two different degradation steps with maxima of absorbance at different wavenumbers. Focusing on the proper wavenumbers (refer to the "Experimental Section" for further details), it is possible to spot the formation of hydrochloric acid,[40] trimethylamine, and acrylate around 300 °C (Figure 4b).[32,41] These molecules are released as gases during the second degradation process as result of the depolymerization of the [2-(acryloyloxy)ethyl]trimethylammonium chloride, thus providing experimental evidence of its presence on the surface of fGO-Step II.

Afterward, electron microscopy was employed to study the morphology of the as-prepared samples, in order to check the uniformity of the active material. **Figure 5** reports a comparison between two active materials. The branched structure of this kind of samples is evident. The GO flakes (Figure 5, right column) are perfectly integrated inside the AC and PVDF networks. In both cases, the absence of aggregation of the polymer clearly demonstrates the effectiveness of the preparation procedure.

Subsequently, Z-potential measurements, performed on the GO and the fGO-Step II samples, confirmed the success of the two-step functionalization procedure. In **Figure 6**, it is possible to appreciate the shift of the peak related to the surface charge of GO flakes. Indeed, starting from −37 mV for the native GO, two peaks are obtained. The positive peak, around 64 mV, is due to the presence of positive charges on the fGO, while the neutral peak, centered in 0 mV, is marking the presence of rGO flakes, reduced but not functionalized during the process. The peak of the pristine GO cannot be identified, meaning that the process was able to convert the nearly totality of GO flakes. This result confirms that the surface charge of the fGO has been properly modified, leading to a shift of the potential of zero charge (V_{PZC}) of the electrode. The electrode in which GO is added will have its V_{PZC} shifted toward positive values, while the electrode in which fGO is added will have its V_{PZC} shifted toward negative values.

**ADVANCED
SCIENCE NEWS**

www.advancedsciencenews.com

**ADVANCED
MATERIALS
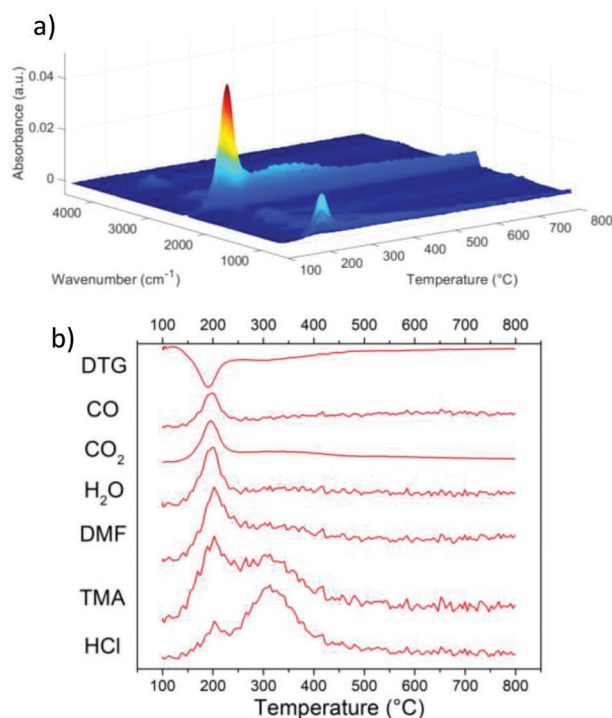TECHNOLOGIES**

www.advmattechnol.de

Figure 4. a) FTIR spectra of the evolved gases during TGA analysis of fGO-Step II versus temperature. b) Infrared adsorption at the maximum adsorption for evaluated molecules compared with DTG.

3.2. Electrochemical Characterization of Materials

Having deeply verified the effectiveness of the functionalization step, electrochemical characterizations were implemented in order to investigate the desalination potentials of the proposed electrodes. Each material employed for CDI was first subjected to CV tests, as described in the "Experimental Section." The results are reported in **Figure 7**. For all the materials, peaks related to hydrogen and oxygen evolution are observed for potentials lower than −0.8 or above +0.6 V (Figure 7a–c), respectively. For positive potentials, the AC with the addition of fGO shows the highest values of specific capacitance, while for negative potentials the AC with the addition of GO is the one with the highest specific capacitance at −0.6 and −0.8 V (Figure 7d). For what concern the Coulombic efficiency, all the materials show a similar behavior (Figure 7e). Following that a device exploiting GO and fGO is expected to show a higher salt adsorption capacitance with respect to a device employing bare activated carbon on both the electrodes. EIS evidenced how the materials show a similar behavior in terms of electrical resistance (Figure 7f). The AC with GO proved to be slightly more resistive than the other two materials, as expected from the shape of the CV curves. To verify the feasibility of coupling of these two electrodes together, 2-electrode CV was performed on the final asymmetric cell, in which the positive electrode was made of AC with fGO, while the negative electrode was made of AC with GO. The CV curves confirm the perfect matching of the two electrodes (Figure 7g). Finally, galvanostatic charge–discharge (Figure 7h) was employed to test the stability over time of the same device. After testing the stability of
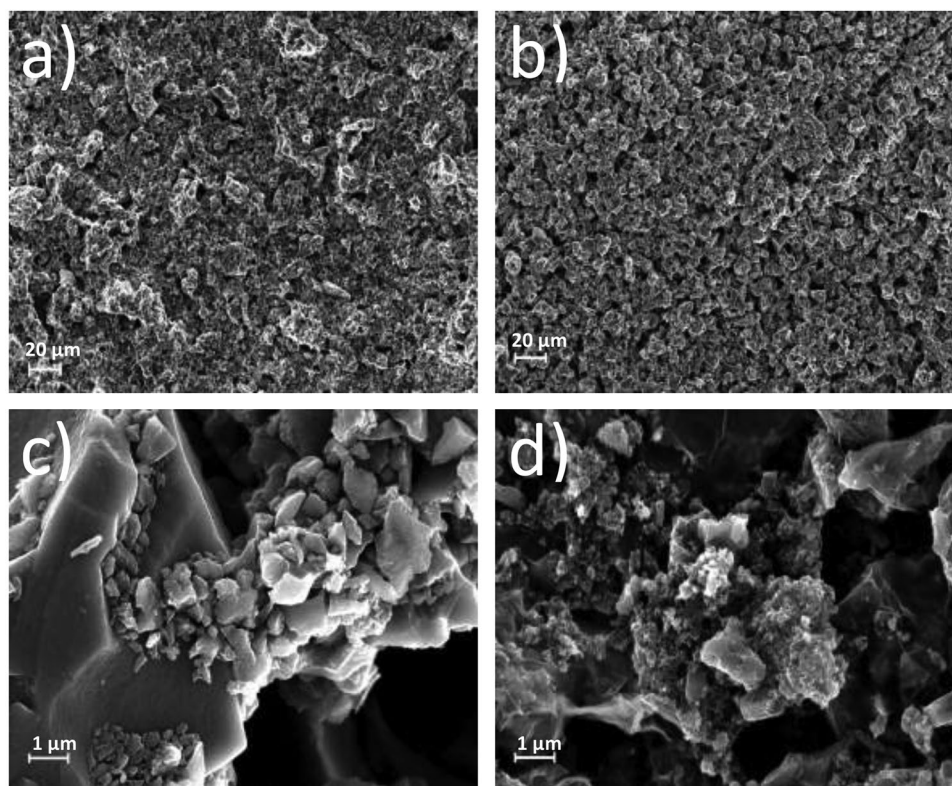

Figure 5. AC and PVDF network—magnification: a) 1000×, c) 25 000×. AC, GO, and PVDF networks—magnification: b) 1000× and d) 25 000×.
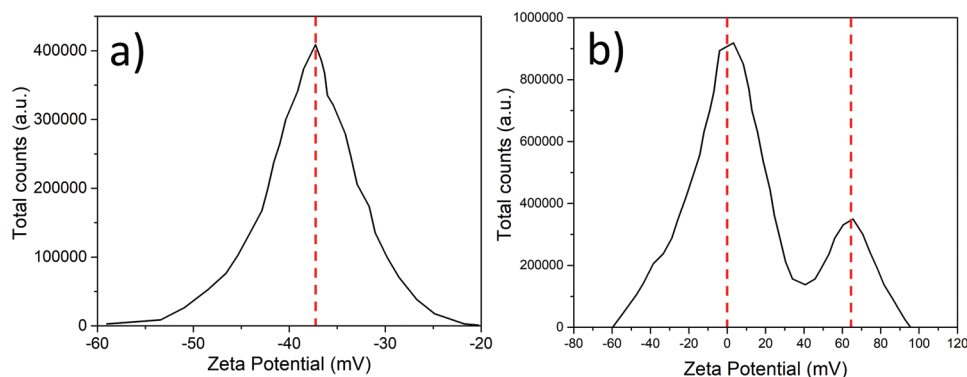
Figure 6. a) Z-potential of GO as it is. The typical negative peak is clearly represented. b) Z-potential of fGO-Step II. Two peaks are present. The positive one is linked to the functionalized flakes (amine). The neutral one, more intense, is related to GO flakes, which have been reduced during the process, but not functionalized.

the materials in this working condition, the voltage window for CDI experiment was set to 1.2 V, the highest potential allowed for aqueous ambient before achieving water electrolysis (1.23 V).

3.3. Capacitive Deionization

In **Figure 8**, the CDI results are reported. In Figure 8a shown is the detail of both the conductivity measured by the conductometer and the current sourced by the potentiostat, plotted as functions of time. In Figure 8b, reported is the amount of adsorbed salt directly evaluated from the data of panel (a). Figure 8c shows the results of the full measurement performed with bare AC on both the electrodes (symmetric electrodes). Figure 8d shows the results of the measurement performed with asymmetric electrodes, in which the negative electrode contains AC and GO, while the positive one contains AC and fGO.

For the symmetric electrodes, a mean mSAC of 11 mg g^{-1} is obtained, with an ASAR of 1.1 mg g^{-1} min^{-1}. The Λ is $\approx$85%. For the asymmetric electrodes, the mean mSAC is 17 mg g^{-1}, the ASAR is 1.7 mg g^{-1} min^{-1}, and the Λ is $\approx$98%. The asymmetric configuration shows better performance. The asymmetric electrodes proved to be able to absorb more salt, more efficiently. To assess the separate contribution of GO and fGO to the overall improvement of desalination performance, two more experiments have been run, combining a neutral electrode (bare AC) with each one of the modified electrodes. Interestingly, the major contribution comes from the fGO. The results are summarized in **Table 1**.

For the sake of a wider perspective, it is necessary to compare these results to the state of the art. Comparing more than 200 values reported in five different reviews,[7,10,11,42,43] it is possible to observe that the majority of the materials show a salt adsorption below 10 mg g^{-1}. Among them, there is a non-negligible portion below 1 mg g^{-1}. The remaining part of the materials shows a salt adsorption of above 10 mg g^{-1}, with just a few above 20 mg g^{-1}. Following that, even if higher performances are reported in literature, an mSAC of 17 mg g^{-1} is a remarkable result.

Suss et al.[12] analyzed more than 100 works previously listed by Zhao et al.[44] and evaluated the Λ for each of them, highlighting that mainly membrane-based capacitive deionization

was able to reach 90% and above. In the present work, we reported a Λ of 98% employing functionalized electrodes, without the need for membranes. The same material, without any functionalization, exhibited a Λ of 85%, proving that the starting material is already showing interesting performances. For the ASAR, instead, a direct comparison with such a vast literature is not available. In this work, the choice of fast charge/discharge CDI cycles (5 min each, 10 min total for a full cycle) provides a final value above 1 mg g^{-1} min^{-1}, which is a remarkable result.

While still interesting to compare the desalination results of the present work with the global CDI scenario, shifting the attention to similar works recently published will provide an in-depth analysis useful to understand the potential of the results obtained in this work. For this purpose, a collection of selected works on highly porous carbons and rGO is listed in **Table 2**. From the past decade it is possible to find works using a great variability of solutions, applied voltages, cell designs, etc. Such choices ended up with different CDI performances, here reported (when available). In details, most of the works reported show an mSAC lower than the one reported in the present work. An exception is the work of Lai et al.[45] reporting a composite of AC and rGO is able to reach an mSAC of 18.6 mg g^{-1} with a Λ of 69%. A year later, Liu and Wang[46] reported a composite of AC and GO showing an mSAC of 22.9 mg g^{-1} for CsCl 20 mg l^{-1}. However, for both of them the CDI cycle was requiring a lot of time, thus lowering the ASAR.

4. Conclusion

We reported a simple and scalable method to obtain a novel functionalized graphene oxide, and we tested this material for capacitive deionization applications. Starting from graphene oxide, a fast two-step process was employed to graft the (2-(acryloyloxy)ethyl)trimethylammonium chloride on its surface. The functionalized graphene oxide obtained in this way has widely been characterized by means of many techniques. To the best of our knowledge, this is the first use of this molecule for CDI applications. The functionalized graphene oxide was mixed with activated carbon. The active material obtained in this way was characterized and tested as
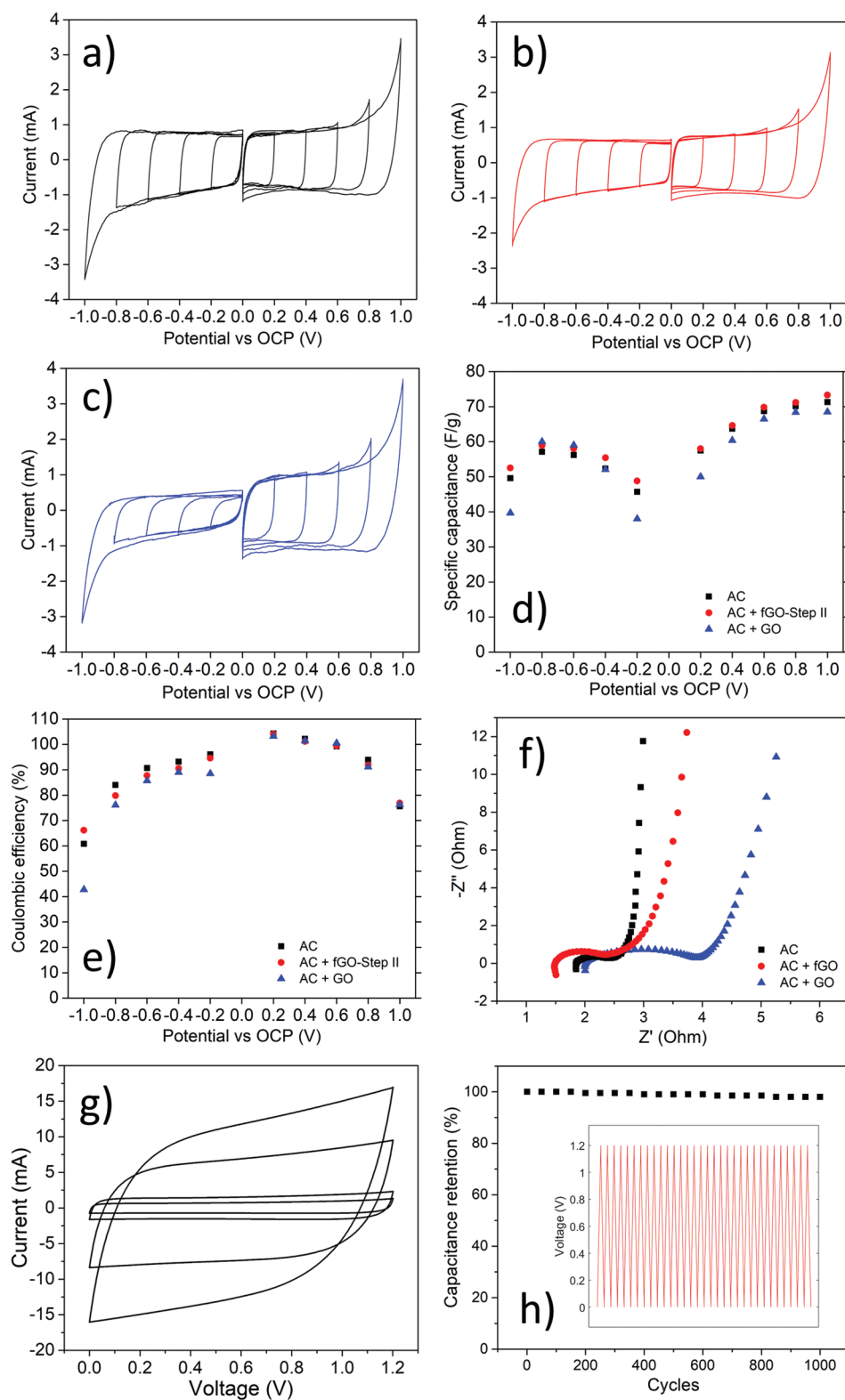
**ADVANCED
SCIENCE NEWS**

www.advancedsciencenews.com

**ADVANCED
MATERIALS
TECHNOLOGIES**

www.advmattechnol.de

Figure 7. Electrochemical characterizations results. a) CV of bare AC. b) CV of AC with fGO-Step II. c) CV of AC with GO. d) Specific capacitance as a function of the applied potential. e) Coulombic efficiency as a function of the applied potential. f) EIS results on the asymmetric cell. Positive electrode: AC + fGO. Negative electrode: AC + GO. g) 2-electrodes' CV on the asymmetric cell. h) Galvanostatic charge–discharge performed on the asymmetric cell.
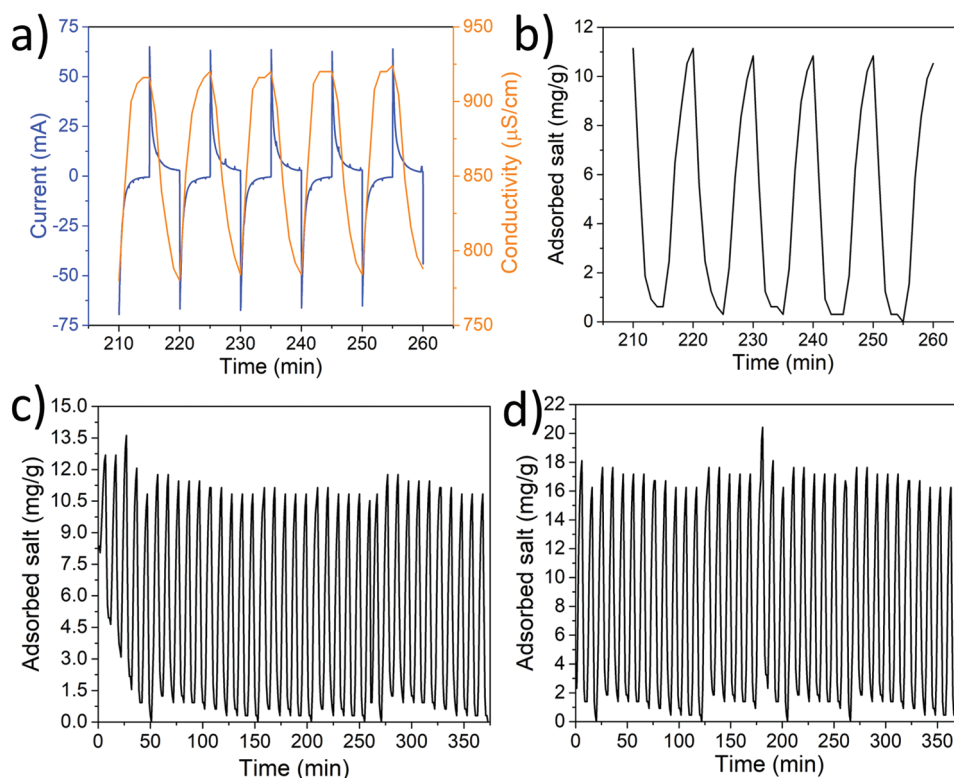
Figure 8. CDI results. a) Details of conductivity and current measurement using symmetric electrodes. b) Details of salt adsorption capacitance of symmetric electrodes. c) Salt adsorption over time using symmetric electrodes. d) Salt adsorption over time using asymmetric electrodes.

Table 1. CDI results for different combinations of materials, reported as maximum salt adsorption capacitance (mSAC), charge efficiency (Λ), and average salt adsorption rate (ASAR).

Positive electrode	Negative electrode	mSAC [mg g^{-1}]	Λ [%]	ASAR [mg g^{-1} min^{-1}]
AC	AC	11 ± 1	85	1.1 ± 0.1
AC	AC + GO	12 ± 1	86	1.2 ± 0.1
AC + fGO	AC	15 ± 1	95	1.5 ± 0.1
AC + fGO	AC + GO	17 ± 1	98	1.7 ± 0.2

Table 2. Comparison of CDI results of various AC and rGO composites recently published.

Material	Solution	Voltage [V]	mSAC [mg g^{-1}]	ASAR [mg g^{-1} min^{-1}]	Λ [%]	Year	Ref.
AC/rGO	NaCl: 0.1 mS cm^{-1}	1.2	2.94	1.76	24	2012	[20]
Meso porous carbon	NaCl: 500 mg L^{-1}	1.6	11.7	0.12	–	2013	[47]
Carbon aerogel/rGO	NaCl: 0.1 mS cm^{-1}	1.2	–	–	59	2014	[21]
AC/rGO	NaCl: 400 mg L^{-1}	1.2	7.2	0.037	–	2014	[48]
rGO	CaCl$_2$: 28.8 mg L^{-1} MgSO$_4$: 22 mg L^{-1} NaHCO$_3$: 39 mg L^{-1}	2.0	3.54	0.16	–	2015	[49]
AC	NaCl: 100 mg L^{-1}	1.2	9.1	0.18	–	2019	[45]
AC/rGO	NaCl: 100 mg L^{-1}	1.2	18.6	0.37	69	2019	[45]
AC/GO	CaCl$_2$: 20 mg L^{-1}	1.2	16.7	0.07	–	2020	[46]
	CsCl: 20 mg L^{-1}		22.9	0.10			
AC	NaCl: 12 µS cm^{-1}	1.8	10^{-3}	10^{-4}	–	2020	[50]
AC/rGO	NaCl: 1200 mg L^{-1}	1.4	8.1	0.27	46	2021	[22]
AC	NaCl: 10 × 10^{-3} м	1.2	11	1.1	85	2021	This work
AC/fGO	NaCl: 10 × 10^{-3} м	1.2	17	1.7	98	2021	This work

**ADVANCED
SCIENCE NEWS**

www.advancedsciencenews.com

**ADVANCED
MATERIALS
TECHNOLOGIES**

www.advmattechnol.de

electrode in a capacitive deionization cell. The results show a high salt adsorption capacitance up to 17 mg g^{-1}, good stability over time, and a notable charge efficiency. These results are comparable with the results reported in literature where costly ion exchange membranes are often employed because of the Donnan potential.[51] The present work provides an in-depth characterization of this novel material, which shows highly promising performances in capacitive deionization. The empirical findings in this study will help shedding light on new materials for CDI, thus paving the road for future scaling-up of the CDI technology.

Future work will focus on the improvement of the negatively charged electrode to further boost the electrosorption capacity. The desalination performance of ion exchange membranes will be compared in the same experimental condition. Furthermore, a study on the viability of employing green solvents will be performed in order to investigate the possibility of avoiding the use of DMF in the functionalization process.

Supporting Information

Supporting Information is available from the Wiley Online Library or from the author.

Conflict of Interest

The authors declare no conflict of interest.

Data Availability Statement

The data that support the findings of this study are available from the corresponding author upon reasonable request.

[1] M. A. Shannon, P. W. Bohn, M. Elimelech, J. G. Georgiadis, B. J. Marinas, A. M. Mayes, *Nature* **2008**, *452*, 301.
[2] Y. Ghalavand, M. S. Hatamipour, A. Rahimi, *Desalin. Water Treat.* **2015**, *54*, 1526.
[3] D. Zhou, L. Zhu, Y. Fu, M. Zhu, L. Xue, *Desalination* **2015**, *376*, 109.
[4] C. K. Diawara, *Sep. Purif. Rev.* **2007**, *37*, 302.
[5] M. K. Wafi, N. Hussain, O. E.-S. Abdalla, M. D. Al-Far, N. A. Al-Hajaj, K. F. Alzonnikah, *SN Appl. Sci.* **2019**, *1*, 751.
[6] M. A. Anderson, A. L. Cudero, J. Palma, *Electrochim. Acta* **2010**, *55*, 3845.
[7] B. Jia, W. Zhang, *Nanoscale Res. Lett.* **2016**, *11*, 64.
[8] P. Ratajczak, M. W. Suss, F. Kaasik, F. Béguin, *Energy Storage Mater.* **2019**, *16*, 126.
[9] Y. H. Teow, A. W. Mohammad, *Desalination* **2019**, *451*, 2.
[10] J. Oladunni, J. H. Zain, A. Hai, F. Banat, G. Bharath, E. Alhseinat, *Sep. Purif. Technol.* **2018**, *207*, 291.
[11] S. Porada, R. Zhao, A. van der Wal, V. Presser, P. M. Biesheuvel, *Prog. Mater. Sci.* **2013**, *58*, 1388.
[12] M. E. Suss, S. Porada, X. Sun, P. M. Biesheuvel, J. Yoon, V. Presser, *Energy Environ. Sci.* **2015**, *8*, 2296.
[13] D. I. Oyarzun, H. Ali, J. W. Palko, M. Stadermann, J. G. Santiago, *Water Res.: X* **2018**, *1*, 100008.
[14] Z. Y. Leong, H. Y. Yang, *ACS Omega* **2020**, *5*, 2097.
[15] X. Che, S. Wang, C. Li, G. Wang, C. Li, S. Wang, D. Li, J. Qiu, *ACS Sustainable Chem. Eng.* **2019**, *7*, 15715.
[16] T. Wu, G. Wang, F. Zhan, Q. Dong, Q. Ren, J. Wang, J. Qiu, *Water Res.* **2016**, *93*, 30.
[17] E. Avraham, M. Noked, I. Cohen, A. Soffer, D. Aurbach, *J. Electrochem. Soc.* **2011**, *158*, 168.
[18] X. Li, B. Zhu, J. Zhu, *Carbon* **2019**, *146*, 320.
[19] A. Boretti, S. Al-Zubaidy, M. Vaclavikova, M. Al-Abri, S. Castelletto, S. Mikhalovsky, *npj Clean Water* **2018**, *1*, 5.
[20] H. Li, L. Pan, C. Nie, Y. Liu, Z. Sun, *J. Mater. Chem.* **2012**, *31*, 15556.
[21] Y. Liu, C. Nie, L. Pan, X. Xu, Z. Sun, D. H. Chua, *Inorg. Chem. Front.* **2014**, *1*, 249.
[22] G. Folaranmi, M. Bechelany, P. Sistat, M. Cretin, F. Zaviska, *Nanomaterials* **2021**, *11*, 1090.
[23] Y. Y. Belaustegui, I. Rincon, F. F. Carretero, P. Azpiroz, A. G. Luis, D. A. Tanaka, *Chem. Eng. J. Adv.* **2021**, *6*, 100094.
[24] I. Roppolo, A. Chiappone, K. Bejtka, E. Celasco, A. Chiodoni, F. Giorgis, M. Sangermano, S. Porro, *Carbon* **2014**, *77*, 226.
[25] I. Cohen, E. Avraham, Y. Bouhadana, A. Soffer, D. Aurbach, *Electrochim. Acta* **2015**, *153*, 106.
[26] S. A. Hawks, A. Ramachandran, S. Porada, P. G. Campbell, M. E. Suss, P. M. Biesheuvel, J. G. Santiago, M. Stadermann, *Water Res.* **2019**, *152*, 126.
[27] R. Zhao, P. M. Biesheuvel, H. Miedema, H. Bruning, A. van der Wal, *J. Phys. Chem. Lett.* **2010**, *1*, 205.
[28] A. Gholampour, M. V. Kiamahalleh, D. N. H. Tran, T. Ozbakkaloglu, D. Losic, *ACS Appl. Mater. Interfaces* **2017**, *49*, 43275.
[29] M. D. Frogley, C. Wang, G. Cinque, A. H. Barber, *Vib. Spectrosc.* **2014**, *75*, 178.
[30] K. Haubner, J. Murawski, P. Olk, M. Lukas, C. Ziegler, B. Adolphi, E. Jahene, *ChemPhysChem* **2010**, *11*, 2131.
[31] C. Xu, R.-s. Yuan, X. Wang, *New Carbon Mater.* **2014**, *29*, 61.
[32] G. Socrates, *Infrared and Raman Characteristic Group Frequencies: Tables and Charts*, Wiley, Chichester, UK **2004**.
[33] SpectraBase, https://spectrabase.com/spectrum/25ZPsqtOQrr (accessed: January, 2022).
[34] G. Durgaprasad, D. N. Sathyanarayana, C. C. Patel, *Bull. Chem. Soc. Jpn.* **1971**, *44*, 316.
[35] SpectraBase, https://spectrabase.com/spectrum/BQ1ZRtgEJi6 (accessed: January, 2022).
[36] SpectraBase, https://spectrabase.com/spectrum/l0LqRdA3ay (accessed: January, 2022).
[37] SpectraBase, https://spectrabase.com/spectrum/G4CBuKNSKtQ (accessed: January, 2022).
[38] SpectraBase, https://spectrabase.com/spectrum/FzvSAmisjBW (accessed: January, 2022).
[39] SpectraBase, https://spectrabase.com/spectrum/bWfQTYHT9x (accessed: January, 2022).

[40] SpectraBase, https://spectrabase.com/spectrum/7sBDgEUj3s (accessed: January, 2022).

[41] SpectraBase, https://spectrabase.com/spectrum/6AQvjnIoTYX (accessed: January, 2022).

[42] M. A. Ahmed, S. Tewari, *J. Electroanal. Chem.* **2018**, *813*, 178.

[43] M. A. Luciano, H. Ribeiro, G. E. Bruch, G. G. Silva, *J. Electroanal. Chem.* **2020**, *859*, 113840.

[44] R. Zhao, P. M. Biesheuvel, A. van der Wal, *Energy Environ. Sci.* **2012**, *5*, 9520.

[45] Y.-T. Lai, W.-T. Liu, L.-C. Chung, P.-I. Liu, M.-C. Chang, R.-Y. Horng, L.-J. Chen, C.-Y. Lee, N.-H. Tai, *Adv. Mater. Technol.* **2019**, *4*, 1900213.

[46] X. Liu, J. Wang, *Sci. Total Environ.* **2020**, *749*, 141524.

[47] G. Wang, B. Qian, Q. Dong, J. Yang, Z. Zhao, J. Qiu, *Sep. Purif. Technol.* **2013**, *103*, 216.

[48] Q. Dong, G. Wang, B. Qian, C. Hu, Y. Wang, Q. Jieshan, *Electrochim. Acta* **2014**, *137*, 388.

[49] T. N. Tuan, S. Chung, J. K. Lee, J. Lee, *Curr. Appl. Phys.* **2015**, *15*, 1397.

[50] O. Sufiani, H. Tanaka, K. Teshima, R. L. Machunda, Y. A. Jande, *Sep. Purif. Technol.* **2020**, *247*, 116998.

[51] A. Hassanvand, K. Wei, S. Talebi, G. Q. Chen, S. E. Kentish, *Membranes* **2017**, *7*, 54.